This a postprint version of the following published document:

Raiola, M., Discetti, S., Ianiro, A. (2015). On PIV random error minimization with optimal POD-based low-order reconstruction. *Experiments in Fluids*, 56(4).

On PIV random error minimization with optimal POD-based low order reconstruction

Marco Raiola · Stefano Discetti · Andrea Ianiro

Abstract Random noise removal from Particle Image Velocimetry data and spectra is of paramount importance, especially for the computation of derivative quantities and spectra. Data filtering is critical, as a trade-off between filter effectiveness and spatial resolution penalty should be found. In this paper a filtering method based on Proper Orthogonal Decomposition and low order reconstruction is proposed. The existence of an optimal number of modes based on the minimization of both reconstruction error and signal withdrawal is demonstrated. A criterion to perform the choice of the optimal number of modes is proposed. The method is first validated via synthetic and real experiments. As prototype problems we consider PIV vector fields obtained from channel flow DNS data and from PIV measurement in the wake of a circular cylinder. We determine the optimal number of modes to be used for the low order reconstruction in order to minimize the statistical random error. The results highlight a significant reduction of the measurement error. Dynamic Velocity Range is enhanced, enabling to correctly capture spectral information of small turbulent scales down to the half of the cutoff wavelength of original data. In addition to this, the capability of detecting coherent structures is improved. The robustness of the method is proved, both for low signal-to-noise ratios and small-sized ensembles. The proposed method can significantly improve the physical insight into the investigation of turbulent flows.

Marco Raiola · Stefano Discetti · Andrea Ianiro
Aerospace Engineering Group, Universidad Carlos III de Madrid, Avenida de la Universidad 30, Leganés 28911, Spain
E-mail: mraiola@ing.uc3m.es

1 Introduction

The key of the success of Particle Image Velocimetry (PIV) lies in its ability to measure the instantaneous velocity simultaneously at several points with sufficient spatial resolution to allow the computation of instantaneous vorticity and rate of strain (Westerweel et al 2013). Unfortunately experimental noise and spuriously detected vectors (commonly referred as outliers) pose great challenges to the reliability of the measurement of gradient-based quantities. For instance, for tomographic PIV measurements, the standard deviation of the divergence computed on raw data of an incompressible flow can be assumed as an estimation of the accuracy of measurement of the velocity spatial derivatives and it is typically found to be around 7% (Ceglia et al 2014) of the maximum vorticity in the measured flow field (locally the error can be much higher). Even using advanced PIV algorithms and temporal filtering of data, a typical figure of 3% error in the vorticity measurements is reported (see, e.g. Violato et al 2012).

PIV measurement uncertainty is traditionally classified in bias and random errors. The bias errors typically appear in the form of peak-locking, i.e. bias towards integer displacement due to the pixel discretization (Westerweel 1997), or as a modulation due to finite spatial resolution effects (Scarano 2003). Even though the bias error received a more significant attention from the community of PIV developers, the random error is often the dominant component of the measurement uncertainty. According to Adrian (1991) the root mean square (rms) of the random error is proportional to the particle image diameter (and hence to the correlation peak width). Other sources of random errors are the change of relative intensity between two exposures of particle images due to out-of-plane motion, fluctuating

background intensity and camera noise introduced during the recording process. Westerweel (2000) reported a typical figure of 0.05 pixels for the rms of the random error. The random error is reported to be highly sensitive to the interrogation procedure: the use of window weighting functions and of advanced interpolators is shown to affect its amplitude (Astarita 2006, 2007). Moreover, false correlation peaks detection mostly occurs when the correlating windows produce an insufficient number of particle image pairs, resulting in the occurrence of spurious vectors (Huang et al 1997). Recognizing and eliminating such incorrect vectors is a mandatory step to obtain undistorted velocity statistics. This procedure is referred as data validation (Westerweel 1994; Westerweel and Scarano 2005).

One path to reduce the instantaneous measurement uncertainty due to random error consists in throwing information from the temporal to the spatial domain. Nowadays the availability of high speed hardware has multiplied the number of attempts in this direction (see the recent works by Cierpka et al 2013; Sciacchitano et al 2012; Novara and Scarano 2013). In three-dimensional flow field measurements physical criteria can be exploited to reduce the measurement uncertainty (see, for instance, the solenoidal filtering approach by Schiavazzi et al 2014). This is normally not possible in planar PIV experiments. In case of non time-resolved data the options to reduce the measurement uncertainty are very limited and often rely simply on spatial filtering which provides a smoother field but, on the downside, a loss of spatial dynamic range.

In this work an approach based on the extraction of a statistical filter from Proper Orthogonal Decomposition (POD, Sirovich 1987) of velocity data ensembles is explored. POD allows for the identification of the flow field principal components. It is possible to extract the instantaneous flow field topology by taking into account a subset of modes containing the bulk of the energy. A low order reconstruction (LOR) acts as a filter on the data while, at the same time, redistributes information from the entire ensemble into the single snapshots, even if they are statistically uncorrelated.

The reconstruction of the flow field with a limited set of POD modes is already a quite assessed instrument for PIV data handling, both for the identification of turbulent coherent structures (Berkooz et al 1993; Adrian et al 2000) and for spurious vectors replacement (Venturi and Karniadakis 2004; Raben et al 2012). In the latter case one can set up criteria based on data smoothness to assess the optimal number of modes (Everson and Sirovich 1995; Raben et al 2012). On the other hand, for data reconstruction, the trade-off between reconstructed signal and noise contamination is still left

to empirical judgment. A common criterion is based on the heuristic consideration that the energy content of the POD-based LOR should be a significative percentage of the energy of the field (Fahl 2000; Ravindran 2000; Bergmann et al 2005). For instance, Liu et al (2001) in a channel flow PIV measurement set a 48% of the turbulent kinetic energy threshold to define the most representative large-scale coherent structures. However, in general, no consideration on the amount of contamination of noise in the reconstructed field is provided, neither the number of modes selected is shown to be optimal.

The choice of the number of modes to obtain an optimal low order reconstruction of noise-corrupted data has been long debated. The filtering capacities of a LOR have been widely investigated in the branches of computers science and data mining (see, e.g. Kargupta et al 2003; Huang et al 2005; Guo et al 2006). On PIV measurements of turbulent flows, instead, the efforts have been focused on the definition and identification of non-corrupted modes more than the identification of an optimality criterion for the reconstruction of the measured flow field (Venturi 2006).

In this paper we propose to use an optimal low order reconstruction to significantly remove random error from PIV data. The parameter for the optimization is the random error minimization. The existence of an optimal number of POD modes for data reconstruction is demonstrated in section 2. An operative criterion for the selection of the optimal number of POD modes is also proposed. The criterion is applied to synthetic data of a DNS channel flow database to validate the method (Section 3). A comparison with commonly-used spatial filtering techniques is also reported in the same section. Finally, a further validation is performed on experimental measurements in the wake of a circular cylinder.

2 Theoretical approach

2.1 The Proper Orthogonal Decomposition

The POD identifies an orthonormal basis for a data matrix using functions estimated as solutions of the integral eigenvalue problem known as Fredholm equation (see Fahl 2000 for a rigorous formulation). Consider a data matrix, that for the case of PIV is the sample ensemble of the fluctuating part of the velocity field according to the Reynolds decomposition, $\underline{\underline{U}} \in \mathbb{R}^{n \times p}$, where n is the number of samples and p is the number of grid points. $\underline{\underline{U}}$ can be decomposed as:

$$\underline{\underline{U}} = \underline{\underline{\Psi}}\,\underline{\underline{\Sigma}}\,\underline{\underline{\Phi}} \tag{1}$$

where $\underline{\underline{\Phi}}$ and $\underline{\underline{\Psi}}$ constitute the decomposition basis of the fluctuating velocity field $\underline{\underline{U}}$, respectively in space and time, and $\underline{\underline{\Sigma}}$ is a diagonal matrix containing the singular values associated to the fluctuating field. The solution is not unique as it depends on the chosen basis functions. POD univocally choses its basis according to a criterion of energy optimality: if we consider $\underline{\underline{U}}$ composed by $\underline{u}_i$ row vectors and $\underline{\underline{\Phi}}$ composed by $\underline{\phi}_j$ row vectors, the objective is a set of $\underline{\phi}_j^\star$ mutually orthonormal vectors satisfying:

$$\left| (\underline{u}_i, \underline{\phi}_j^\star) \right| = \max_{\|\underline{\phi}_j\|=1} \frac{1}{n} \sum_{i=1}^{n} \left| (\underline{u}_i, \underline{\phi}_j) \right| \tag{2}$$

where (a, b) and $\|a\|$ indicate respectively the ℓ^2 inner product and its associated norm in the vector space. The solution to this problem is given by the normalized eigenmodes of the two-point spatial covariance matrix:

$$\underline{\underline{U}}^T \underline{\underline{U}} = \underline{\underline{\Phi}}^T \underline{\underline{\Sigma}} \underline{\underline{\Sigma}} \underline{\underline{\Phi}} = \underline{\underline{\Phi}}^T \underline{\underline{\Lambda}} \underline{\underline{\Phi}} \tag{3}$$

Sirovich (1987, snapshot method) demonstrated that the POD modes can be calculated as the eigenmodes of the two-point temporal covariance matrix:

$$\underline{\underline{U}} \underline{\underline{U}}^T = \underline{\underline{\Psi}} \underline{\underline{\Sigma}} \underline{\underline{\Sigma}} \underline{\underline{\Psi}}^T = \underline{\underline{\Psi}} \underline{\underline{\Lambda}} \underline{\underline{\Psi}}^T \tag{4}$$

Since $\underline{\underline{U}} \underline{\underline{U}}^T$ is a non-negative Hermitian matrix, it has a complete set of non-negative eigenvalues, whose magnitude indicates the energy contribution of the respective eigenmodes. In the snapshot method implementation the number of eigenvalues is equal to that of the snapshots, while the maximum number of non-zero positive eigenvalues is equal to the rank of $\underline{\underline{U}}$. As the eigenmodes are ordered by their energy contribution, the field reconstructed with the first k most energic modes is given by:

$$\underline{\underline{U}}_k = \underline{\underline{\Psi}} \begin{pmatrix} \underline{\underline{I}}_k & \underline{0} \\ \underline{0} & \underline{0} \end{pmatrix} \underline{\underline{\Sigma}} \underline{\underline{\Phi}} = \underline{\underline{\Psi}} \begin{pmatrix} \underline{\underline{I}}_k & \underline{0} \\ \underline{0} & \underline{0} \end{pmatrix} \underline{\underline{\Psi}}^T \underline{\underline{U}} \tag{5}$$

where $\underline{\underline{U}}_k$ is the reconstructed flow field, $\underline{\underline{I}}_k$ indicates the rank k identity matrix and $\underline{0}$ indicates that the matrix containing $\underline{\underline{I}}_k$ is a square matrix of dimension $n \times n$ with zero entries except for $\underline{\underline{I}}_k$.

2.2 Reconstruction optimum

In this section we propose a theory on optimal low order reconstruction from POD modes. From now on the concept of optimality of the reconstruction will be associated to the minimization in the reconstruction of random errors that affects the raw data. The effect of bias error is not taken into account in this analysis and it is totally out of the scope of this work.

The fluctuating part of the measured flow field ensemble $\underline{\underline{\widetilde{U}}}$ can be decomposed in the sum of a random error part $\underline{\underline{E}}$ and an objective function $\underline{\underline{U}}$. From now on, symbols signed with a tilde refer to measured quantities, while symbols unsigned refers to objective function quantities. The objective function $\underline{\underline{U}}$ is not the exact fluctuating component of the velocity field, as it is affected by the bias errors. However, since these errors are related mostly to peak locking effects and to finite spatial resolution, it can be assumed that they depend on the limits of the processing algorithm, and thus cannot be removed by a filter. The measured flow field is:

$$\underline{\underline{\widetilde{U}}} = \underline{\underline{U}} + \underline{\underline{E}} \tag{6}$$

The sample covariance matrix is:

$$\underline{\underline{\widetilde{U}}} \underline{\underline{\widetilde{U}}}^T = \underline{\underline{U}} \underline{\underline{U}}^T + \underline{\underline{U}} \underline{\underline{E}}^T + \underline{\underline{E}} \underline{\underline{U}}^T + \underline{\underline{E}} \underline{\underline{E}}^T \tag{7}$$

As it can be assumed that the random error is uncorrelated with the objective field, considering a Gaussian error with standard deviation σ and provided that the number of vectors is sufficiently large, according to Huang et al (2005), the sample covariance matrix is approximately equal to:

$$\underline{\underline{\widetilde{U}}} \underline{\underline{\widetilde{U}}}^T \approx \underline{\underline{U}} \underline{\underline{U}}^T + p\sigma^2 \underline{\underline{I}}_n \tag{8}$$

where σ is the standard deviation of the random error. For a non-Gaussian (but still independent and identically distributed) error the approximation is still valid when the matrix $\underline{\underline{\widetilde{U}}}$ is rectangular, so that all the eigenvalues of $\underline{\underline{E}} \underline{\underline{E}}^T$ are with high probability in a neighborhood of σ (Marchenko and Pastur 1967). This is formally equal to assume a spectrally white distribution of the random error part in the eigenvalues of the covariance matrix. A proof of the validity of this hypothesis will be given in section 3.1.

Recalling that the POD solves the eigenproblem for the sample covariance matrix in both perturbed and unperturbed cases:

$$\begin{cases} (\underline{\underline{U}} \underline{\underline{U}}^T + p\sigma^2 \underline{\underline{I}}_n \quad \widetilde{\lambda}_j \underline{\underline{I}}_n) \underline{\widetilde{\psi}}_j = 0 \\ \qquad (\underline{\underline{U}} \underline{\underline{U}}^T \quad \lambda_j \underline{\underline{I}}_n) \underline{\psi}_j = 0 \end{cases} \tag{9}$$

It is possible to conclude that:

$$\begin{cases} \widetilde{\lambda}_j \approx \lambda_j + p\sigma^2 \quad \Rightarrow \underline{\underline{\widetilde{\Lambda}}} \approx \underline{\underline{\Lambda}} + p\sigma^2 \underline{\underline{I}}_n \\ \underline{\widetilde{\psi}}_j \approx \underline{\psi}_j \qquad \Rightarrow \underline{\underline{\widetilde{\Psi}}} \approx \underline{\underline{\Psi}} \end{cases} \tag{10}$$

These relationships can be more accurately derived from matrix perturbation theory, along with their bounds, and are a common assumption in perturbed Principal Component Analysis (PCA) applications (Kargupta

et al 2003; Huang et al 2005). This approximation is correct if the random errors are small with respect to the distance between two succesive eigenvalues of $\underline{U}\,\underline{U}^T$ (Stewart 2001; Kargupta et al 2003; Venturi 2006). The perturbation of the eigenvectors increases as λ approaches the value of σ.

If we indicate with $\underline{\widetilde{U}}_k$ the reconstruction of measured flow field with the first k components, considering Eq. 5 and Eq. 6, the difference between the objective field and $\underline{\widetilde{U}}_k$ modes is:

$$
\begin{aligned}
\underline{U}\quad\underline{\widetilde{U}}_k &= \underline{\widetilde{\Psi}}\,\underline{I}_n\,\underline{\widetilde{\Psi}}^T\,\underline{U}\quad\underline{\widetilde{\Psi}}\begin{pmatrix}\underline{I}_k & \underline{0}\\ \underline{0} & \underline{0}\end{pmatrix}\underline{\widetilde{\Psi}}^T(\underline{U}+\underline{E})\\
&= \underline{\widetilde{\Psi}}\begin{pmatrix}\underline{0} & \underline{0}\\ \underline{0} & \underline{I}_{n\ k}\end{pmatrix}\underline{\widetilde{\Psi}}^T\,\underline{U}\quad\underline{\widetilde{\Psi}}\begin{pmatrix}\underline{I}_k & \underline{0}\\ \underline{0} & \underline{0}\end{pmatrix}\underline{\widetilde{\Psi}}^T\,\underline{E}
\end{aligned}
\tag{11}
$$

and considering Eq. 10 :

$$
\begin{aligned}
&(\underline{U}\quad\underline{\widetilde{U}}_k)(\underline{U}\quad\underline{\widetilde{U}}_k)^T\\
&= \underline{\widetilde{\Psi}}\begin{pmatrix}\underline{0} & \underline{0}\\ \underline{0} & \underline{I}_{n\ k}\end{pmatrix}\underline{\widetilde{\Psi}}^T\,\underline{U}\,\underline{U}^T\,\underline{\widetilde{\Psi}}^T\begin{pmatrix}\underline{0} & \underline{0}\\ \underline{0} & \underline{I}_{n\ k}\end{pmatrix}\underline{\widetilde{\Psi}}\\
&\quad+ \underline{\widetilde{\Psi}}\begin{pmatrix}\underline{I}_k & \underline{0}\\ \underline{0} & \underline{0}\end{pmatrix}\underline{\widetilde{\Psi}}^T\,\underline{E}\,\underline{E}^T\,\underline{\widetilde{\Psi}}^T\begin{pmatrix}\underline{I}_k & \underline{0}\\ \underline{0} & \underline{0}\end{pmatrix}\underline{\widetilde{\Psi}}\\
&= \underline{\Psi}\begin{pmatrix}\underline{0} & \underline{0}\\ \underline{0} & \underline{I}_{n\ k}\end{pmatrix}\underline{\Lambda}\,\underline{\Psi}^T + \underline{\Psi}\begin{pmatrix}\underline{I}_k & \underline{0}\\ \underline{0} & \underline{0}\end{pmatrix}p\sigma^2\,\underline{\Psi}^T
\end{aligned}
\tag{12}
$$

By using the linearity and rotation invariance of the trace of a tensor:

$$
\begin{aligned}
&\mathrm{Tr}\Big((\underline{U}\quad\underline{\widetilde{U}}_k)(\underline{U}\quad\underline{\widetilde{U}}_k)^T\Big)\\
&= \mathrm{Tr}\left(\begin{pmatrix}\underline{0} & \underline{0}\\ \underline{0} & \underline{I}_{n\ k}\end{pmatrix}\underline{\Lambda}\right) + \mathrm{Tr}\left(\begin{pmatrix}\underline{I}_k & \underline{0}\\ \underline{0} & \underline{0}\end{pmatrix}p\sigma^2\right)\\
&= \sum_{i=k+1}^{n}\lambda_i + \sum_{i=1}^{k}p\sigma^2 = \sum_{i=k+1}^{n}\lambda_i + kp\sigma^2
\end{aligned}
\tag{13}
$$

Using the Frobenius norm, we define the reconstruction error δ_{RT} with respect to the true flow field as:

$$
\begin{aligned}
\delta_{RT}(k) &= \left(\frac{1}{np}\right)^{\frac{1}{2}}\|\underline{U}\quad\underline{\widetilde{U}}_k\|_F\\
&= \left(\frac{1}{np}\mathrm{Tr}\Big((\underline{U}\quad\underline{\widetilde{U}}_k)(\underline{U}\quad\underline{\widetilde{U}}_k)^T\Big)\right)^{\frac{1}{2}}
\end{aligned}
\tag{14}
$$

Substituting Eq. 13 into the error expression:

$$
\delta_{RT}(k) = \left(\frac{1}{np}\right)^{\frac{1}{2}}\left(\sum_{i=k+1}^{n}\lambda_i + kp\sigma^2\right)^{\frac{1}{2}}
\tag{15}
$$

Due to its optimality properties, the POD spectrum will always decade faster or at least with the same rate of the spectrum in another non-optimal base, the
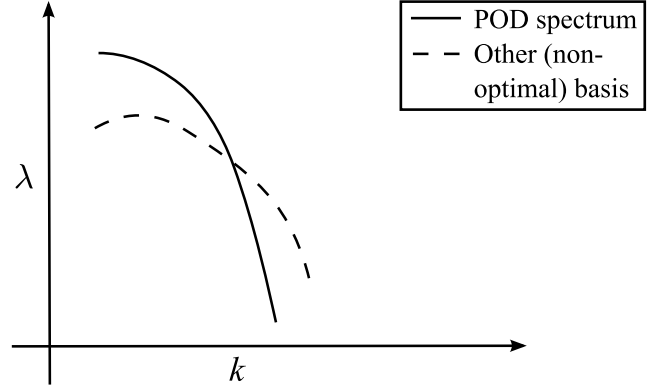

Fig. 1: POD spectrum and another non-optimal basis spectrum for a dissipative system. Adopted from Berkooz et al (1993).

Fourier spectrum for instance. This concept is well represented in Fig.1, adapted from Berkooz et al (1993). We can then hypothesize that POD's eigenvalues decay rate can be modeled in a conservative way with that of a turbulent spectrum in the Fourier space. For instance, in the inertial subrange:

$$
\lambda_i = Ci^{\frac{5}{3}}
\tag{16}
$$

where C is a proportionality constant. To evaluate it, one can consider that the sum of the λ_i is equal to the total kinetic energy in the ensemble:

$$
\sum_{i=1}^{n}\lambda_i = \sum_{i=1}^{n}Ci^{\frac{5}{3}} = npq \Rightarrow C \approx \frac{npq}{\zeta(5/3)}
\tag{17}
$$

where q is the turbulent kinetic energy averaged over all the spatio-temporal data ensemble and $\zeta(s)$ is the Euler-Riemann zeta function. Substituting Eq. 16 and Eq. 17 into Eq. 15, discrete deriving δ_{RT} with respect to k and equating to zero:

$$
\begin{aligned}
\frac{\Delta\delta_{RT}(k^\star)}{\Delta k} &= 0\\
&\Downarrow\\
\sum_{i=k^\star+1}^{n}\lambda_i\quad\sum_{i=k^\star}^{n}\lambda_i + p\sigma^2 &= \frac{npq}{\zeta(5/3)}k^{\star\frac{5}{3}} + p\sigma^2 = 0
\end{aligned}
\tag{18}
$$

It is easy to notice that $k^\star$ is a minimum point as $\frac{\Delta^2}{\Delta k^2}\delta_{RT} > 0$. The optimum number of modes to reconstruct the field, i.e. the one that minimizes the random errors, is:

$$
k^\star = \left(\frac{nq}{\sigma^2\zeta(5/3)}\right)^{\frac{3}{5}}
\tag{19}
$$

In general the effective $k^\star$ corresponds to a lower number of modes than indicated in Eq. 19 due to POD optimality with respect to the ℓ^2 norm. However, in principle in experimental applications the standard deviation of the random error is not known a priori; furthermore the Eq. 19 is a direct consequence of assuming the POD eigenvalues decaying as in the inertial subrange of a high Reynolds number turbulent flow. Consequently, Eq. 19 spotlights the existence of an optimal number of modes, but it has very limited practical applicability. That relation gives a clear description of the $k^\star$ dependencies: it increases both with the ratio of the turbulent kinetic energy and the random error energy and with the number of samples in the ensemble.

Even if Eq. 19 cannot be used to choose $k^\star$, it can be used to safely estimate the number of samples required for the convergence of the proposed method. Suppose that the objective is a noise reduction by a factor RF (i.e. the residual error energy in the reconstructed fields is $(1-RF)\sigma^2$). Since the noise spectral distribution is white, the relation $n \approx (1-RF)^{-1}k^\star$ is a reasonable approximation. Then, from Eq. 19:

$$n \approx (1-RF)^{-\frac{5}{2}}\left(\frac{q}{\sigma^2\zeta(5/3)}\right)^{\frac{3}{2}} \tag{20}$$

The required number of samples can be assessed via a prior approximate estimate of the q and of the expected measured random error.

In order to find an operative criterion for the choice of the optimal number of modes to be retained, the reconstruction error with respect to the measured field can be considered:

$$\delta_{RM}(k) = \left(\frac{1}{np}\right)^{\frac{1}{2}}\|\underline{\tilde{U}} - \underline{\tilde{U}}_k\|_F$$
$$= \left(\frac{1}{np}\right)^{\frac{1}{2}}\left(\sum_{i=k}^{n}\lambda_i + (n-k)p\sigma^2\right)^{\frac{1}{2}} \tag{21}$$

Consider the relative decrease rate of the reconstruction error δ_{RM}, here called $F(k)$, defined as the ratio between forward and backward discrete derivative of $\delta_{RM}^2(k)$:

$$F(k) = \frac{\delta_{RM}^2(k+1)-\delta_{RM}^2(k)}{\delta_{RM}^2(k)-\delta_{RM}^2(k-1)} = \frac{\lambda_k + p\sigma^2}{\lambda_{k-1}+p\sigma^2} \tag{22}$$

The quantity in Eq. 22 may reach asymptotically 1, for k sufficiently large. In the next section it will be shown that a reasonable threshold for the number of modes to retain can be set at $F(k^\star) = 0.999$. This is formally equivalent to look for an elbow in δ_{RM}, and can be considered a restatement of the classic *scree test plot* (Cattell 1966) used in PCA to determine the number of components to retain in a low order reconstruction.

3 Validation

3.1 Numerical validation on synthetic images

Synthetic images are generated from the DNS database of channel flow at Reynolds number equal to 4000 (based on the bulk velocity U_b and twice the half-channel height h) included in the John Hopkins Turbulence Database (Li et al 2008; Yu et al 2012; Graham et al 2013). The DNS domain size is $8\pi h \times 2h \times 3\pi h$. The data are stored in a $2048 \times 512 \times 1536$ points grid. For the purpose of the PIV synthetic experiment bi-dimensional square sub-domains with one side corresponding to the wall, covering regions with size $h \times h$ and parallel to x-y plane are extracted from the DNS domain. These sub-domains are used to generate synthetic images with dimensions 1024×1024 pixels (resulting in a resolution of 4 pixels/grid DNS points). The displacements are multiplied by a scaling factor in order to achieve a mean displacement on the channel centerline equal to 15 pixels.

Gaussian particles (mean diameter 3 pixels, standard deviation 0.5 pixels, 300 counts peak intensity) are randomly generated with a particle density of 0.01 particles per pixel. The laser intensity is simulated to be Gaussian (with half power width equal to 4 pixels along the thickness of the light sheet) in order to take into account the effect of correlation degradation due to the out-of-plane motion. Noise with uniform distribution (maximum intensity 50 counts, standard deviation 14.4 counts) is added on the images.

The interrogation strategy is an iterative multi-step image deformation algorithm, with final interrogation windows of 32x32 pixels, 75% overlap. A Blackman weighting window is used to improve the stability and the spatial resolution (Astarita 2007). Vector validation is carried out with a universal median test (Westerweel and Scarano 2005) on a 3x3 vectors kernel and threshold equal to 2 is used to identify invalid vectors. Discarded vectors are replaced with a distance-weighted average of neighbor valid vectors. The spatial resolution achieved in this simulated experiment is realistic and consistent with that of recent PIV experiments (see, e.g. Hong et al 2012 achieving a resolution of about 125×60 vectors in a $2h \times h$ domain). The standard deviation of the random error σ is estimated by interrogating images with zero-imposed displacement and same background noise feature, and it is found to be equal to 0.18 pixels. The mean turbulent kinetic energy q in the ensemble is of about 1.29 square pixels.

According to Eq. 20, in order to aim to a target of random error reduction of 80%, 8000 synthetic images are generated to form the ensemble. With the same val-
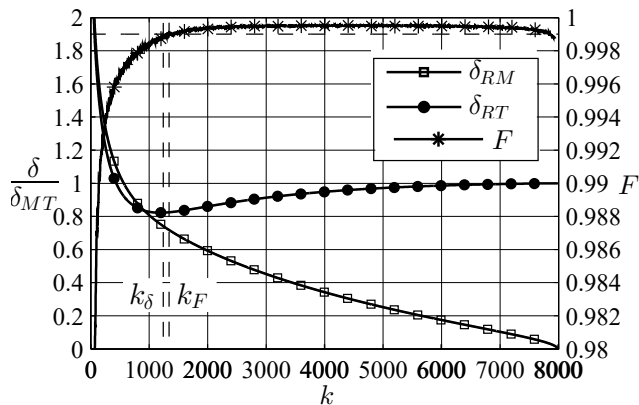
Fig. 2: δ_{RT}, δ_{RM} (left axis) and F (right axis) versus the number of modes used in the reconstruction.

Fig. 3: POD eigenvalues over the firsts 4000 modes. Note that error includes both bias and random part.

ues, the expected optimal number of modes $k^\star$ (Eq. 19) is of about 1300 modes. The 8000 images are obtained by using flow fields with a time separation equal to 250 DNS timesteps (corresponding, in our resolution, to a displacement of 250 pixels on the channel centerline) and with a space separation along the z direction equal to $0.23h$ (235 pixels). The flow fields are taken at two streamwise positions, i.e. $x = 0$ and $x = 4\pi h$. The number of images is doubled by flipping data from the other half of the channel.

In Fig. 2 the values of $\delta_{RT}(k)$ and $\delta_{RM}(k)$ as defined by Eq. 14 and Eq. 21 are plotted; data are presented in non-dimensional form dividing by δ_{MT}, i.e. the error of the measured field with respect to the true one, that in this test is equal to 0.32 pixels. It has to be outlined here that this value is higher than the random noise since it includes also signal modulation and other bias errors. The minimum δ_{RT} is reached when the first 1200 modes are used for the reconstruction (corresponding to 96.6% of the fluctuating energy of the measured field). The effective number of modes which minimize the reconstruction error will be indicated with k_δ. It has to be remarked that a quite extended plateau of about 500 modes width is present, thus the exact choice of the number of modes to be retained is not critical, provided that one can identify a reasonable estimate of the range in which the optimum should be. In this plateau the error is of about $0.82\ \delta_{MT}$ (corresponding to a 0.06 pixels total error reduction). Beyond 1200 modes δ_{RM} has approximately a linear trend with k. Indeed, as noise has a white spectral distribution, it is reasonable to expect that for large k the contribution of each mode is approximately constant. The relative decrease rate of the reconstruction error $F(k)$ defined in Eq. 22 is also plotted; its values are low-pass filtered (windowed linear-phase FIR digital filter with 25 points span and
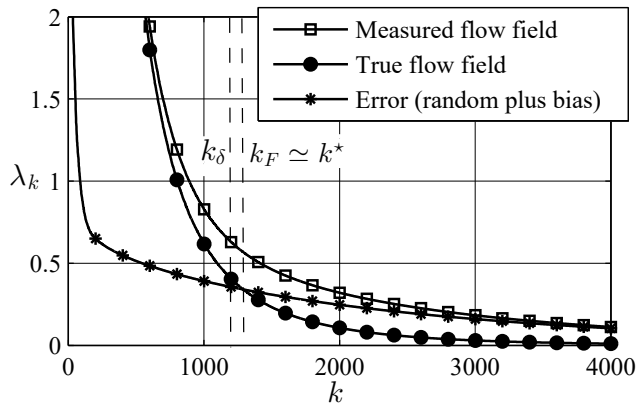
normalized cutoff frequency 0.0313). The relative decrease rate of the reconstruction error approaches 1 beyond 1200 modes, apart from the very last coefficients in which the linearity of the contribution of noise is lost. A reasonable threshold is $F(k) = 0.999$, corresponding to $k \approx 1300$ and to a δ_{RT} nearby the minimum. The number of modes satisfying the relation $F(k) = 0.999$ will be referred from now on with the symbol k_F.

In Fig. 3 the POD spectra of the measured and true flow fields and of the error are illustrated. The latter is defined as the difference between measured and true flow fields, thus it includes both bias and random part of the error. The eigenvalues of both measured and true fields follow approximately a power law, at least for the first half of the set of POD modes. The eigenvalues of the error present a slower decay rate. Even if this may seem in contrast with the hypothesis introduced in section 2.2, i.e. white random error distribution, it should be remarked that, in the plot, the error includes also bias. It is worth to highlight that true spectrum and error spectrum cross over in the region that contains the values $k^\star$, k_δ and k_F. After the cross over point, the measured spectrum approaches error spectrum. This means that, from this point on, each additional mode included in the reconstruction would introduce a contribution in which noise is predominant on the signal.

In Fig. 4 a true snapshot is compared to the raw snapshots obtained with PIV interrogation and with POD-based low order reconstruction (LOR). Maps of the out-of-plane vorticity component are reported to stress differences. The measured field (Fig. 4c) is affected by spurious vortical features that are not present in the original field. As an example, the negative vorticity peak marked as A in the figure is much weaker in the original field, while in the measured field has intensity comparable to that of the vortex marked as
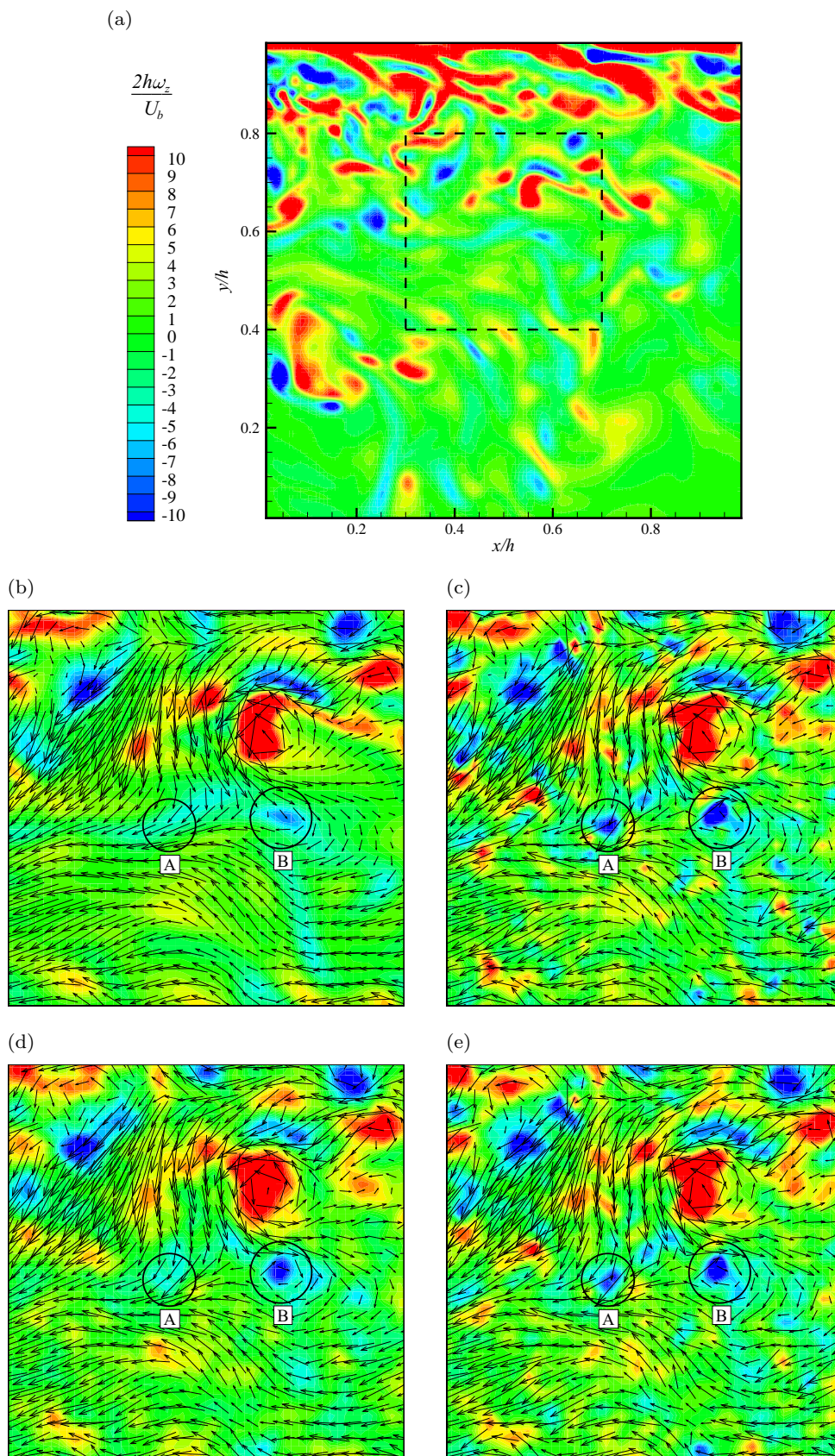
(a)

(b)

(c)

(d)

(e)

Fig. 4: Instantaneous fluctuating vorticity (ω_z) field. a) The DNS field used for this benchmark. Magnified view of the: b) DNS field, c) measured field, d) field reconstructed with 1300 modes, e) field reconstructed with 3000 modes.
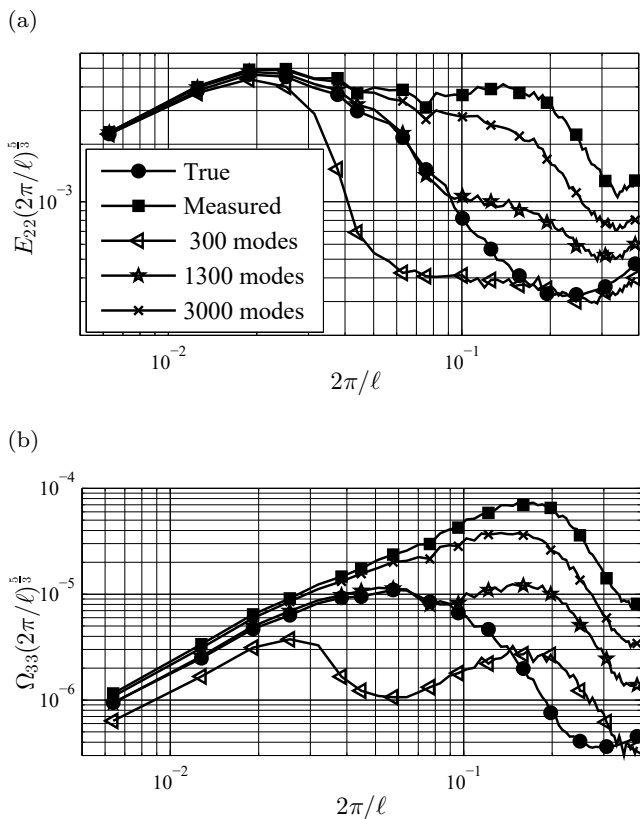
(a)

(b)

Fig. 5: a) Compensated transverse velocity spectra E_{22} in stream-wise direction versus wavelength ℓ; b) transverse vorticity spectra Ω_{33} in stream-wise direction versus wavelength ℓ.

B, that is an original field feature. The optimal reconstruction with 1300 modes (Fig. 4d) provides an astonishing improvement of the data quality with respect to the measured field. This reconstruction smears out the negative vorticity peak in A, while retaining vortex B. Such a result could not be achieved by a conventional spatial filter as it will be shown in subsection 3.3. Even though the residual error $\delta_{RT}(k_\delta)$ from Fig. 2 might still appear relatively large, it has to be reminded that in this simulated experiment the measurement error is dominated by bias due to finite spatial resolution. If the number of modes used for the low order reconstruction is significantly increased (e.g. 3000 modes in Fig. 4e) the noise contamination is stronger, and, for instance, the vortex A is still present.

In Fig. 5 the power spectra of the true, the measured and the reconstructed fields are reported. In both Fig. 5a and 5b the wavelengths are expressed in pixels. Data are proposed in Fig. 5a in the form of the compensated spectrum (i.e. multiplied by the wavenumber to the 5/3) in order to magnify the effects at the smallest scales. It has to be remarked that, even in the case

of the original DNS data, the spectrum at the small scales is contaminated by aliasing effects due to the finite length of the domain. The reconstruction with 1300 modes closely follows the DNS spectral behavior to a larger extent with respect to reconstructions with a larger number of modes. The growth of the error with respect to the true spectrum for smaller wavelengths can be associated mostly to the residual noise. For the sake of completeness, the spectrum obtained by a reconstruction with a lower number of modes is also reported. The reconstruction with 300 modes (which corresponds to 95% of the fluctuating energy) causes a significant underestimation of the spectral energy of a wide range of large scales, thus highlighting that the information obtained from these modes is still insufficient to achieve a proper description of the flow field. The vorticity spectra reported in Fig. 5b further stress the improvement achieved using the optimal POD filter. The spectrum obtained using 1300 modes for the reconstruction follows with high fidelity the true one up to a wavelength of 70 pixels. The spectrum obtained from the PIV measured data largely overestimate the vorticity power spectrum already at very large scales (e.g. 35% at 512 pixels and 100% at 128 pixels) due to the measurement noise. The LOR with only 300 modes provides a completely distorted view of the vorticity distribution over the turbulent scales (even if taking into account the 95% of the energy content).

3.2 Validation of the criterion for modes selection

In the subsection 3.1 relative decrease rate of the reconstruction error $F(k)$ was shown to be a possible parameter to be used for the choice of the optimal number of k modes to be used for the LOR, being $F(k) = 0.999$ a suitable threshold value. This criterion is here assessed on synthetic images for several conditions, by changing the parameters affecting $k^\star$ as given by Eq. 19 (i.e. the number of snapshots used in the POD n and the standard deviation of the random noise σ). A study to evaluate the effects of a change of resolution on the selection criterion is also performed. It will be shown in the following that the spatial resolution is not an independent parameter, since it effects both q, σ and also the maximum number of images to be used in the POD.

The effect of a lower number of images (6000 images in Fig. 6 and 4000 in Fig. 7) is tested under the same noise level and resolution of the test case in section 3.1. Figs. 6a-7a show that the number of modes that minimize the error k_δ decreases with n decreasing, in agreement with the trend predicted by Eq. 19. The weaker reduction of k_δ with respect to the theoretical
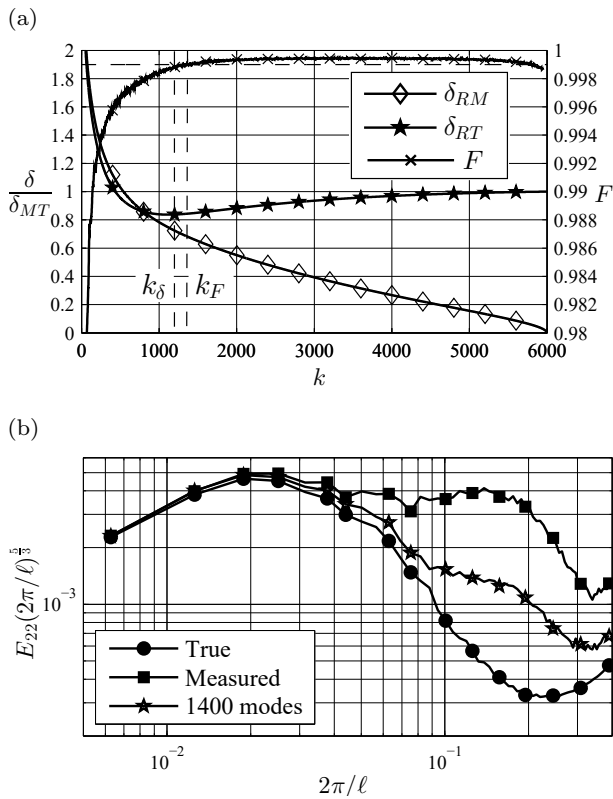
(a)

(a)

(b)

(b)

Fig. 6: 6000 images test case: a) δ_{RT}, δ_{RM} (left axis) and F (right axis) versus the number of modes used in the reconstruction; b) Compensated transverse velocity spectra E_{22} in stream-wise direction versus wavelength ℓ reconstructed with k_F number of modes.

Fig. 7: 4000 images test case: a) δ_{RT}, δ_{RM} (left axis) and F (right axis) versus the number of modes used in the reconstruction; b) Compensated transverse velocity spectra E_{22} in stream-wise direction versus wavelength ℓ reconstructed with k_F number of modes.

prediction of Eq. 19 can be associated to the hypothesis of POD spectrum equal to the Fourier spectrum introduced for simplification in section 2. The flatness of the curve δ_{RT} is also affected by a smaller number of snapshots: the maximum achievable error reduction decreases, while the plateau centered in k_δ increases in size. This behavior is consistent with a lower degree of separation between true field and noise modes, that produces a stronger contamination of the measured field modes. The values of k_F track the k_δ value in a conservative way (with respect to preserving the signal content), always predicting a number of modes slightly larger than k_δ. Difference between k_F and k_δ increases as the ensemble decreases in size. This is mainly due to an increase in the extension of the optimal plateau and affects only marginally the reconstruction: the value k_F estimated with the $F(k) = 0.999$ criterion always identifies a δ_{RT} inside the optimal plateau, i.e. a low order reconstruction with an error nearly equal to the optimal one. The effect of a smaller ensemble size on velocity spectra is shown in Fig. 6b and 7b, respectively for $n = 6000$ and $n = 4000$ snapshots. The low order
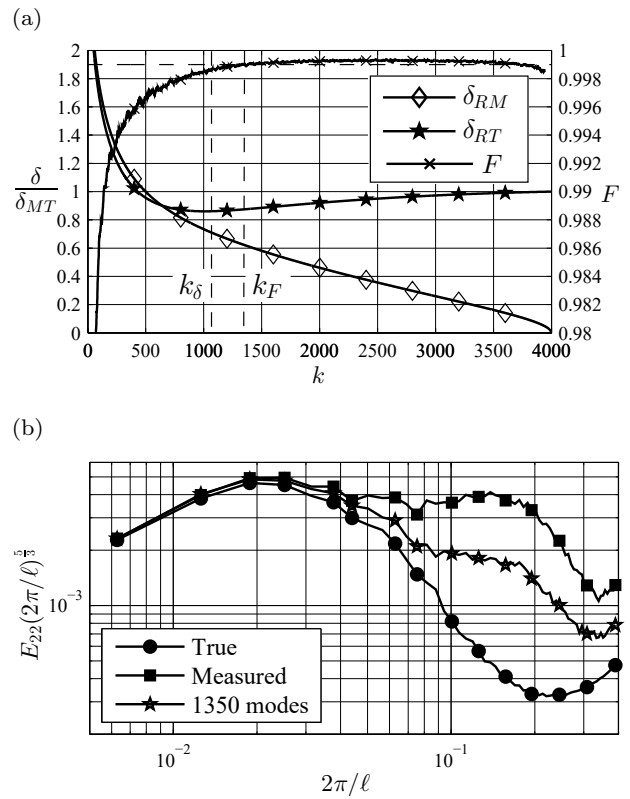
reconstruction obtained with the $F = 0.999$ criterion is less effective in predicting the true spectrum as the ensemble size decreases, but it still achieves remarkable results (reduction of about 75% and 40% of the original error for a 64 pixels wavelength, respectively for $n = 6000$ and $n = 4000$).

Fig. 8 and 9 show the effect of a change in the level of background noise. The intensity of the uniformly distributed noise is set to 25 ad 75 counts (the original case was generated with 50 counts noise), leading respectively to $\sigma = 0.11$ and $\sigma = 0.27$ pixels (estimated with zero-displacement test) on the calculated velocity fields. Resolution and number of images are set as in the test case of subsection 3.1. A lower level of noise (Fig. 8a) shifts the k_δ value towards an higher number of modes, meaning that it is possible to achieve an higher order reconstruction without introducing strongly corrupted modes. Conversely, an higher noise level (Fig. 9a) shifts k_δ towards a lower number of modes, meaning that noise is significantly contaminating a larger spectrum of modes. As in the previous case, the variation of k_δ respects the trend predicted by Eq. 19. It should
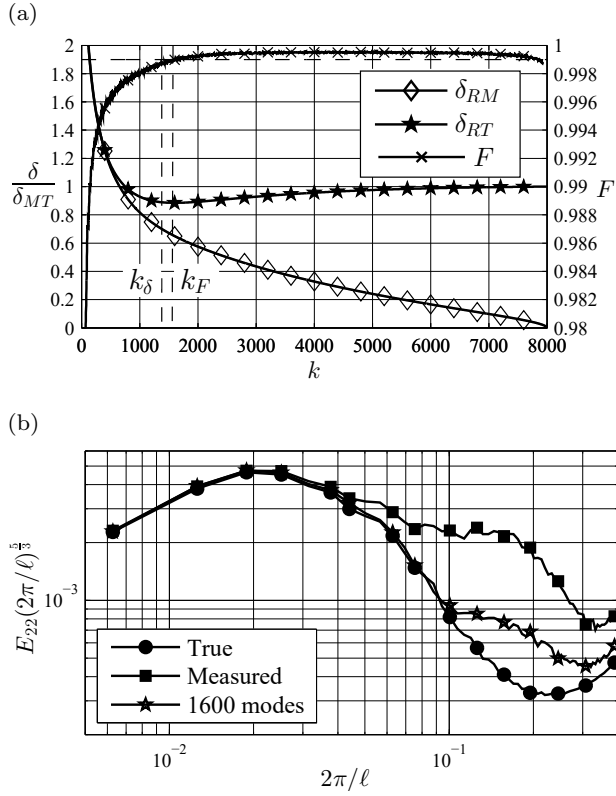
(a)

(a)

(b)

(b)

Fig. 8: $\sigma = 0.11$ test case: a) δ_{RT}, δ_{RM} (left axis) and F (right axis) versus the number of modes used in the reconstruction; b) Compensated transverse velocity spectra E_{22} in stream-wise direction versus wavelength ℓ reconstructed with k_F number of modes.

Fig. 9: $\sigma = 0.27$ test case: a) δ_{RT}, δ_{RM} (left axis) and F (right axis) versus the number of modes used in the reconstruction; b) Compensated transverse velocity spectra E_{22} in stream-wise direction versus wavelength ℓ reconstructed with k_F number of modes.

be highlighted that the δ_{RT} curve shape is strongly affected by the noise level: the maximum percentual noise reduction increases when the noise level increases, while the optimal plateau extension decreases. The $F(k) = 0.999$ criterion permits a reasonable prediction of the k_δ position with a conservative weak overestimation, still achieving a value of δ_{RT} inside the optimal plateau. For lower noise levels the LOR obtained with the $F = 0.999$ criterion achieves a lower percentual noise reduction with a larger k_F. The effect of this behavior on velocity spectra is shown in Fig. 8b: a lower percentage of energy is discarded, while the higher order reconstruction leads to a more precise computation of the spectra (predicted spectrum is extremely accurate up to a 64 pixels wavelength). In Fig. 9b the effect of a more intense noise contention on velocity spectrum is shown. Less favorable cases permit to discard an higher percentage of noise-related fluctuation energy, at the cost of a poorer, but still satisfying description of the spectrum (reduction of the 85% of the original error for a 64 pixels wavelength).
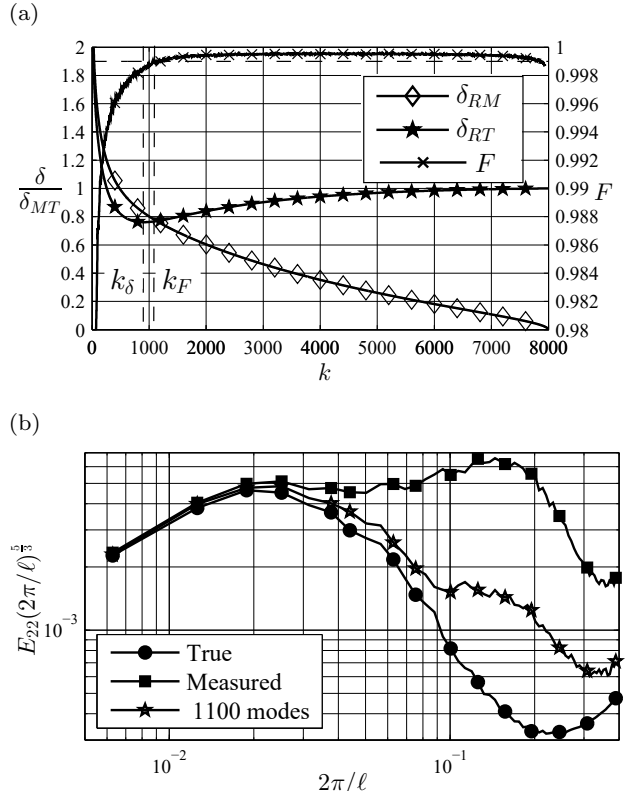
As previously reported in subsection 2.1, the maximum number of modes of the POD is given by the rank of the vector field $\underline{U}$, meaning that the maximum number of images n that can be used in the POD snapshot method is limited by the velocity field grid points p, i.e. by the PIV algorithm final resolution. This means that it is not possible to change the spatial resolution without modifying also the number of images used for POD and the noise level. A test is performed on the PIV images used for the basic test case, changing the final interrogation window to 32x32 pixel with 50% overlap (Fig. 10). For this test case a $q = 1.32$ square pixels and a $\sigma = 0.17$ pixels are estimated, while the number of images used for the POD has been reduced to 3900. It is difficult in this case to extract information that a change in resolution produces on the estimate of k_δ, since effects of a change of both noise level and number of snapshots should be taken into account. As in the previous cases, also for this case the $F = 0.999$ criterion predicts an overestimation of k_δ, and a $\delta_{RT}(k_F)$ value completely inside the optimal plateau. The main effect that can be distinguished is a reduction of the

(a)

(b)

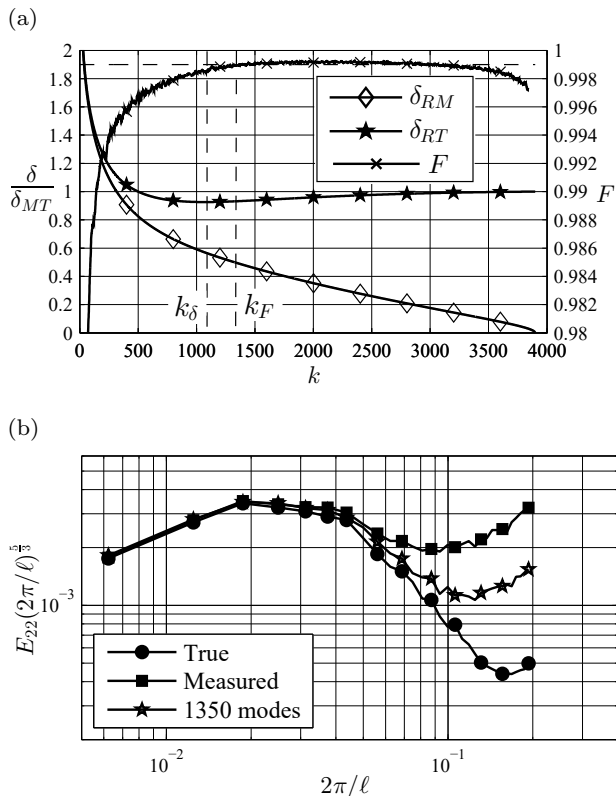Fig. 10: Lower spatial resolution test case: a) δ_{RT}, δ_{RM} (left axis) and F (right axis) versus the number of modes used in the reconstruction; b) Compensated transverse velocity spectra E_{22} in stream-wise direction versus wavelength ℓ reconstructed with k_F number of modes.
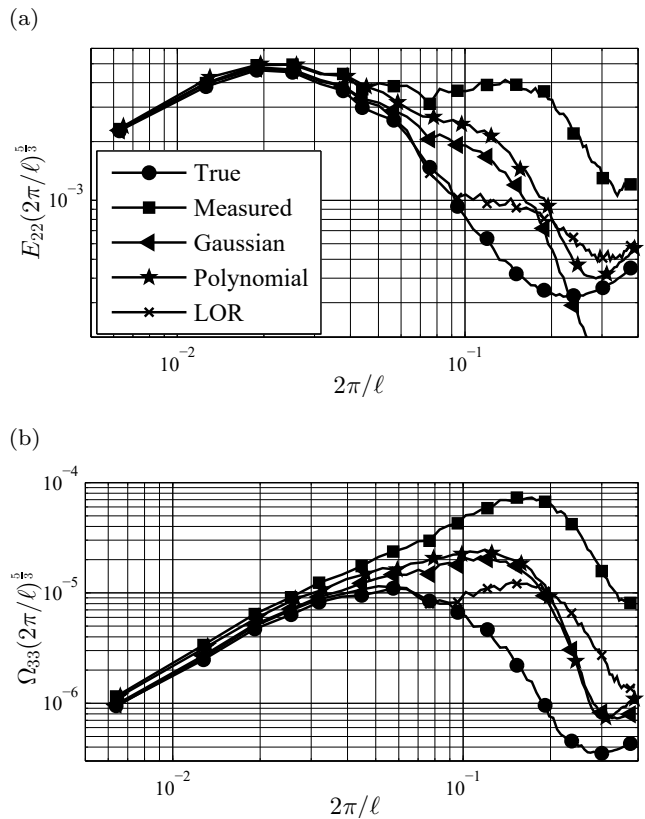
(a)

(b)

Fig. 11: Spatial filter comparison: a) Compensated transverse velocity spectra E_{22} in stream-wise direction versus wavelength ℓ; b) transverse vorticity spectra Ω_{33} in stream-wise direction versus wavelength ℓ.

maximum error reduction with respect to the case with 4000 images (Fig. 7a) that seems to be at least partially justified by a reduction of the noise level and an increment of average turbulent kinetic energy. The velocity spectrum reconstructed with k_F number of modes (Fig. 10b) still gives remarkable results (the error reduction for a 64 pixels wavelength is higher than 60% of the original error).

3.3 Comparison with spatial filtering

In this subsection the performances of the proposed optimal low order reconstruction are compared with those of standard spatial filtering techniques. The test case is the same of subsection 3.1. In Fig. 11 the velocity and vorticity spectra of the LOR with 1300 modes are compared with those of two of the most commonly adopted spatial filtering techniques found in PIV literature: Gaussian filter (kernel size 5x5 grid points, corresponding to ±3 standard deviations) and second order

polynomial filter (kernel size 5x5 grid points). The low order reconstruction (LOR) outperforms the standard spatial filtering techniques, achieving a precise description of both velocity and vorticity spectra up to a 70 pixel wavelength. For the velocity spectrum at the same wavelength the Gaussian filter and the polynomial filter provide respectively an error reduction of 65% and 40% with respect to the original error. A similar behavior is observed on the vorticity spectra.

Direct comparison of istantaneous vorticity fields (Fig. 12) clarifies the astonishing performance of the optimal POD-based LOR with respect to conventional spatial filters. As anticipated in subsection 3.1, optimal LOR (Fig. 12b) is capable to retain true field vortical features (such as the vortex labeled as A) and to discard spurious vortical features (such as the vortex labeled as B) even if the intensities of these features are quite similar. Conversely, in the same context, both Gaussian filter and polynomial filter (respectively Figs. 12c-12d) retain both true field and spurious vortical features.
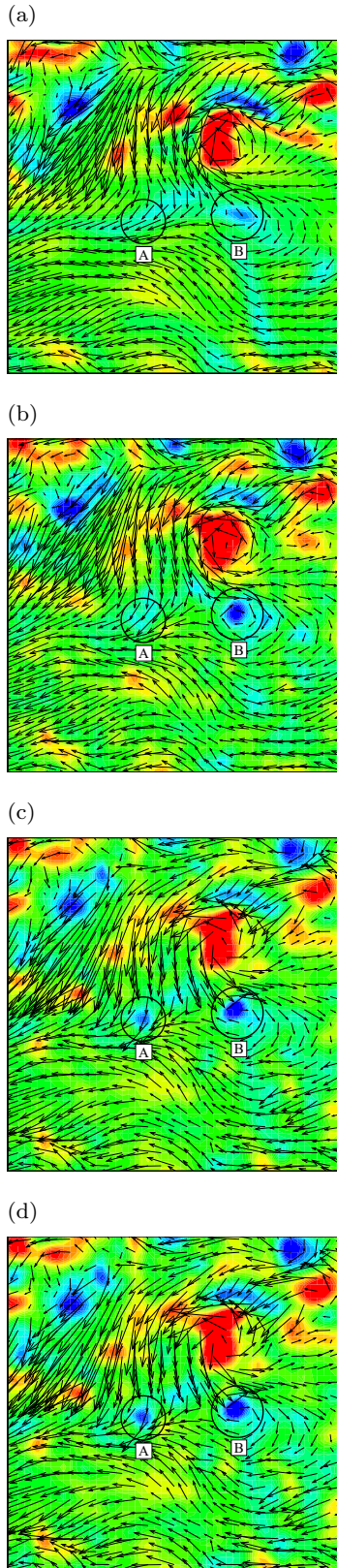
Fig. 12: Instantaneous fluctuating vorticity (ω_z) field. Magnified view of the: a) DNS field, b) field reconstructed with 1300 modes, c) field filtered with Gaussian filter, d) field filtered with polynomial filter.

3.4 Experimental validation

The POD-based filter is validated on an experimental PIV dataset. The flow field under investigation is the turbulent wake of a infinite circular cylinder.

The experiment is performed in the recirculating wind tunnel of the Aerospace Engineering Group at University Carlos III of Madrid. The wind tunnel has a square test section of 400 mm height. Free stream turbulence intensity is estimated to be lower than 1%. A circular cylinder, with diameter $D = 10$ mm, is mounted at tunnel's half height, spanning the entire test section width. The blockage ratio is equal to 0.025. The free stream velocity U_∞ at the end of the contraction is about 6.2 m/s which gives a Reynolds number based on the cylinder diameter of about 3900.

The flow is seeded with Di-Ethyl-Hexyl-Sebacat droplets with diameter of approximately 1 μm. The light source is a Big Sky Laser CFR400 ND:Yag (230 $mJ/pulse$). The acquisition is performed with two Andor Zyla 5.5MP sCMOS cameras (2560×2160 $pixels$ resolution, 16.6×14.0 mm sensor size). The cameras are synchronized in order to grab images simultaneously. The first camera is equipped with a 25 mm focal length objective. The resolution of the images grabbed with the first camera is equal approximately to 55 pix/D (5.5 pix/mm). The second camera is equipped with a Nikon 60 mm focal length objective. The resolution of the images grabbed with the second camera is equal approximately to 110 pix/D (11 pix/mm). The time delay between laser pulses is chosen to be 200 μs, in order to give a displacement of about 14 $pixels$ in the higher resolution images and of about 7 $pixels$ in the lower resolution images. The higher resolution camera has then a lower relative error, since the measured displacement is longer while the expected absolute error is the same (the typical figure of merit of 0.1 $pixels$, Adrian and Westerweel 2011). The velocity fields grabbed from the higher resolution camera are considered to be the reference fields due to their intrinsically lower noise content (Neal et al 2015), while the corresponding velocity fields grabbed from the lower resolution camera are the measurement on which POD-based filtering is performed. The cameras are placed side by side in order to have an overlap region between their respective field of view of about 14 cylinder diameters. An optical calibration is performed on both the cameras as described in Heikkila (2000). Using the calibration parameters, dewarping is applied to the two cameras images in order to match the overlap region as in Giordano et al (2012). The overlap regions of both images are dewarped on the same grid (size 1548×443 $pixels$) with resolution equal to 110 pix/D (11 pix/mm). The PIV interrogation strat-
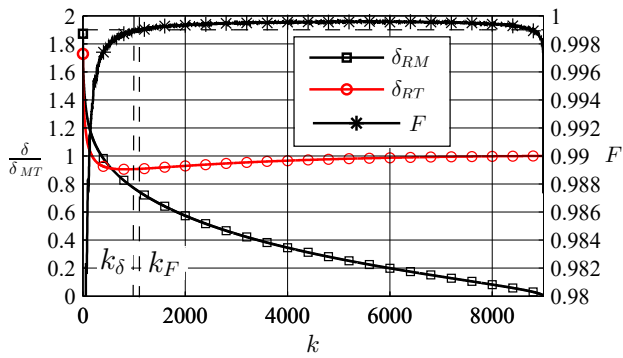
Fig. 13: δ_{RT}, δ_{RM} (left axis) and F (right axis) versus the number of modes used in the reconstruction.

Fig. 14: Compensated transverse velocity spectra E_{22} in stream-wise direction versus wavelength ℓ.

egy is an iterative multistep image deformation algorithm with final interrogation window of 32×32 $pixels$ and 75% overlap. The Blackman weighting windows is used in the cross-correlation step (Astarita 2007). The vector validation (universal median test, 5×5 kernel, threshold 2) is implemented similarly to the synthetic testcase. The processed images result in 190×52 velocity vectors fields. The POD-based filter is applied on an ensemble of 9000 velocity fields grabbed from the lower resolution camera.

The values of $\delta_{RM}(k)$, $\delta_{RT}(k)$ and of the function $F(k)$ (low-pass filtered by windowed linear-phase FIR digital filter with 25 points span and normalized cut-off frequency 0.0313) are plotted in Fig.13. The reconstruction errors $\delta_{RM}(k)$ and $\delta_{RT}(k)$ are presented in non-dimensional form, normalized by the error of the measured field over the true field δ_{MT}, that for this test is equal to 1.29 $pixels$. Compared with the previous synthetic benchmarks, a similar shape in the error both with respect to the measured flow field $\delta_{RM}(k)$ and with respect to the true flow field $\delta_{RT}(k)$ is found. The minimum δ_{RT} is reached for $k_\delta \approx 1000$ (corresponding to 84.7% of the fluctuating energy of the measured field). As in the synthetic benchmark, in this test an extended plateau is present around the value k_δ, in which the function δ_{RT} has a nearly constant value of about 0.9 δ_{MT}. By taking as a criterion a value of $F(k^\star) = 0.999$, an optimum number of modes $k_F \approx 1100$ is found. For a number of modes higher than k_F, the error δ_{RM} has a nearly linear trend that indicates a dominant contribution of random noise in the reconstruction.

In Fig. 14 the power spectra of the true, the measured and the reconstructed velocity fields are reported. Data are plotted in the form of the compensated spectrum (i.e. multiplied by the wavenumber to the 5/3) in order to magnify the effects at the smallest scales; wavelengths are expressed in pixels. Wavelengths smaller than 64 pixels are not considered in the comparison.
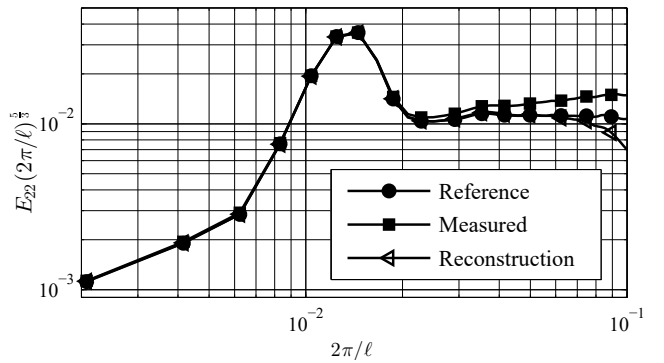
This limit deposed to account for the filtering behavior of the PIV algorithm itself, that degrades spectral information at scales comparable to the interrogation window size. The reconstruction with 1100 modes closely follows the reference field spectral behavior nearly up to the limit considered in the comparison, sightly underestimating the spectral power (4% error at 90 $pixels$). The spectrum obtained from non-filtered data, instead, considerably overestimates the reference spectrum even at large scales (14% at 160 $pixels$ and 25% at 90 $pixels$) due to its noise content.

The direct comparison of raw, filtered and reference fluctuating velocity fields (Fig. 15) gives a better insight on the noise removal obtained using the POD-based filter. The raw measured flow field (Fig. 15c) is degraded by measurement noise if compared to the reference field (Fig. 15a). A number of spurious vectors are present in the measured field, and even some large scales flow structures appears to be distorted and barely recognizable. The POD-filtered velocity field (Fig. 15b) is smoother and more regular than both measured field (Fig. 15c) and reference field (Fig. 15a). This behavior is twofold: indeed one should consider that the reference field itself is a measurement, meaning that it contains some measurement uncertainty and thus noise. Moreover the POD-filter is able to recover coherent structures in the field and save them from being smeared out in the filtering process. While this certainly happens for large structures that are well discretized, this is not likely to happen to poorly discretized structures due to the nature of the proposed method, that looks for a trade-off between field description and noise removal. This behavior can be better appreciated in the velocity spectrum (Fig. 14), where the POD reconstruction appears to overfilter the smaller scales.
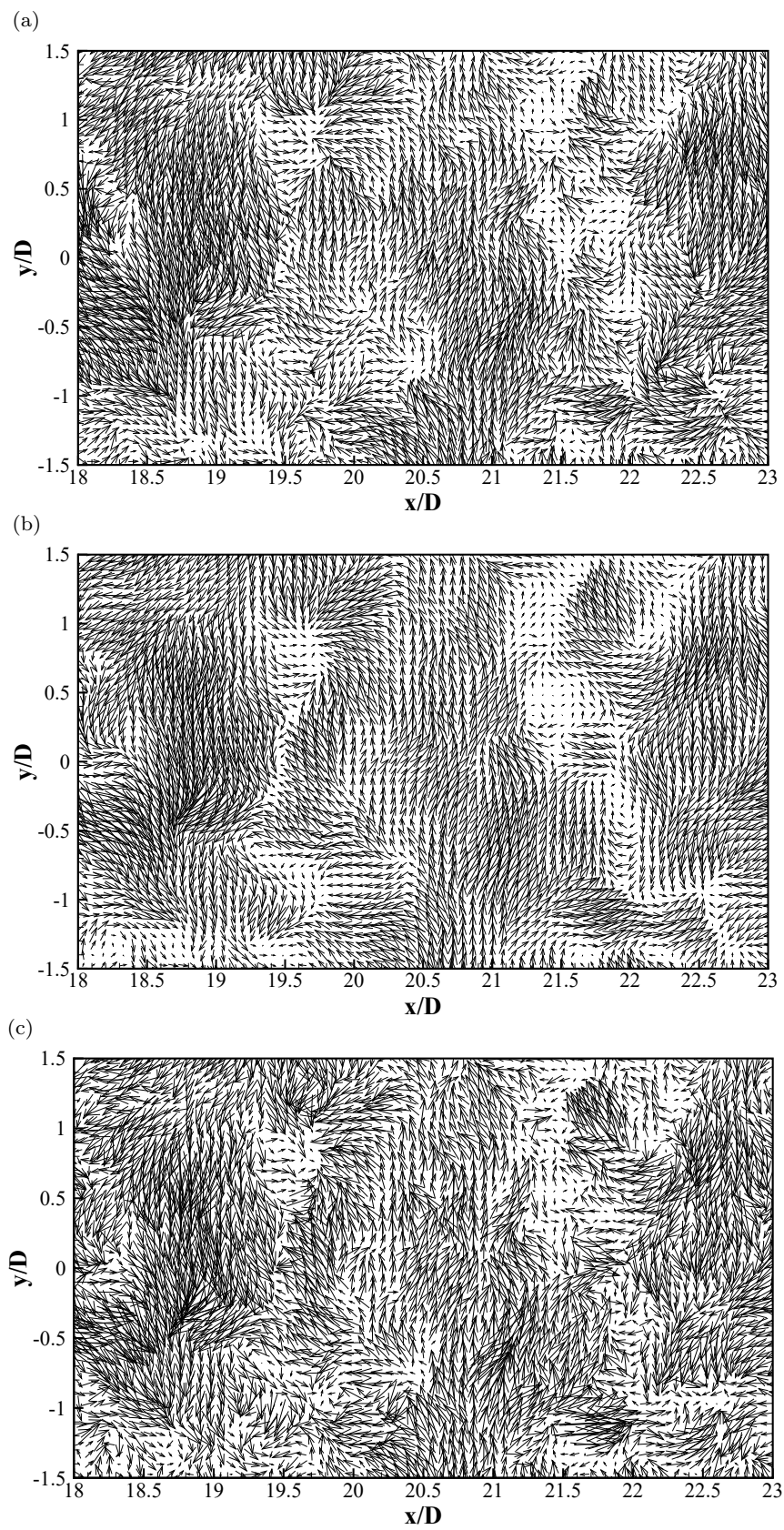
(a)

(b)

(c)

Fig. 15: Magnified view of fluctuating velocity fields: a) reference velocity field, b) velocity field reconstructed with 1100 POD modes, c) measured velocity field.

4 Conclusion

The existence of an optimal number of POD modes to achieve random error minimization in low order reconstruction of randomly perturbed flow fields (such as PIV data) is demonstrated. The reduction of the random error is extremely beneficial in the computation of derivative quantities, which are more prone to be affected by noise amplification. An empirical criterion for the choice of the optimal number of modes is also indicated and validated. The optimal number of modes is obtained by simply observing the variation of the difference between the reconstructed fields and the original ones, without adding any hypothesis on the features of the flow field itself, thus making the method very robust and flexible. Notwithstanding with the relatively low sensitivity of random error on the optimal number of modes (thus simplifying the task of finding an empirical criterion), for the first time a robust method is provided without relying on computation of the retained energy in the reconstructed fields. The method is validated on synthetic images ensembles generated from a channel flow DNS data set and on real PIV measurements in the wake of a circular cylinder. In the first test case the error is dominated by modulation effects, which cannot be recovered by the POD-based low order reconstruction. Nevertheless, a total error reduction of about 18% is achieved, corresponding to a value that is about the 33% of the noise estimated with a zero-displacement benchmark test, while retaining most of the spectral information of the original field. The vorticity distributions highlight that the method is able to suppress spurious vorticity blobs without removing original vortical structures with comparable size and intensity. The spectra of the data closely follow those of the DNS for a wider portion of the wavelengths with respect to reconstruction with a larger number of modes. The cutoff wavelength is slightly larger than twice the interrogation window size. In the experimental testcase a total error reduction of about 10% in respect to the reference field is achieved. The velocity spectrum of the low order reconstruction reveals that noise reduction preserves small scale structures up to scales comparable with the interrogation window size. Furthermore, the low order reconstruction is very effective in removing clusters of spurious vectors, which generally pose a challenge to the standard validation methods. An extensive parametric validation with synthetic test cases is performed, proving the robustness of the method and of the criterion used for the identification of the optimal low order reconstruction. Moreover the method allows for improvements: more efficient predictions are obtained in more favorable cases (high signal-to-noise ratio and large ensemble). As expected, the improvement is more remarkable on derivative quantities (see, for instance, the vorticity spectra). Comparison with common spatial filtering techniques provides a clear idea of the advantages that this technique could introduce, especially for measurement of turbulence statistics. The proposed method is expected to contribute in enhancing the reliability of PIV as it allows for uncertainty reduction and robustness improvement. The spatial resolution might also indirectly benefit from it. Indeed, generally the choice of the processing algorithm (window size, interrogation method, etc.) arises from a trade-off between desired spatial resolution and measurement noise amplification. The optimal low order reconstruction allows for the use of advanced high resolution interrogation algorithms since the random noise can be consistently reduced in post-processing. As turbulent flows investigation is demanding in terms of dynamic range requirements, this advancement would be beneficial.

References

Adrian RJ (1991) Particle-image techniques for experimental fluid mechanics. Annu Rev Fluid Mech 23:261–304

Adrian RJ, Westerweel J (2011) Particle image velocimetry. 30, Cambridge University Press

Adrian RJ, Christensen KT, Liu ZC (2000) Analysis and interpretation of instantaneous turbulent velocity fields. Exp Fluids 29:275–290

Astarita T (2006) Analysis of interpolation schemes for image deformation methods in piv: Effect of noise on the accuracy and spatial resolution. Exp Fluids 40:977–987

Astarita T (2007) Analysis of weighting windows for image deformation methods in piv. Exp Fluids 43:859–71

Bergmann M, Cordier L, Brancher JP (2005) Optimal rotary control of the cylinder wake using proper orthogonal decomposition reduced-order model. Phys Fluids 17:097101, DOI http://dx.doi.org/10.1063/1.2033624

Berkooz G, Holmes P, Lumley JL (1993) The proper orthogonal decomposition in the analysis of turbulent flows. Annu Rev Fluid Mech 25:539–575

Cattell RB (1966) The scree test for the number of factors. Multivar Behav Res 1:245–276

Ceglia G, Discetti S, Ianiro A, Michaelis D, Astarita T, Cardone G (2014) Three-dimensional organization of the flow structure in a non-reactive model aero engine lean burn injection system. Experimental Thermal and Fluid Science 52:164–173

Cierpka C, Lütke B, Kähler CJ (2013) Higher order multi-frame particle tracking velocimetry. Exp Fluids 54:1–12, DOI 10.1007/s00348-013-1533-3

Everson R, Sirovich L (1995) Karhunenloeve procedure for gappy data. J Opt Soc Am 12:165764

Fahl M (2000) Trust-region methods for flow controlbased on reduced order modeling. Phd dissertation, Trier University, Trier, Germany

Giordano R, Ianiro A, Astarita T, Carlomagno GM (2012) Flow field and heat transfer on the base surface of a finite circular cylinder in crossflow. Applied Thermal Engineering 49:79–88

Graham J, Lee M, Malaya N, Moser R, Eyink G, Meneveau C, Kanov K, Burns R, Szalay A (2013) Turbulent channel flow data set, available at http://turbulence.pha.jhu.edu/docs/README-CHANNEL.pdf

Guo S, Wu X, Li Y (2006) On the lower bound of reconstruction error for spectral filting based privacy preserving data mining. In: In Proceedings of the 10th European Conference on Principles and Practice of Knowledge Discovery in Databases, Berlin, Germany

Heikkila J (2000) Geometric camera calibration using circular control points. Pattern Analysis and Machine Intelligence, IEEE Transactions on 22(10):1066–1077

Hong J, Katz J, Meneveau C, Schultz M (2012) Coherent structures and associated subgrid-scale energy transfer in a rough-wall turbulent channel flow. J Fluid Mech 712:92–128, DOI 10.1017/jfm.2012.403

Huang HT, Dabiri D, Gharib M (1997) On errors of digital particle image velocimetry. Meas Sci Technol 8:142740

Huang Z, Du W, Chen B (2005) Deriving private information from randomized data. In: In Proceeding of the ACM SIGMOD Conference of Management of Data, Baltimore, BA

Kargupta H, Datta S, Wang Q, Sivakumar K (2003) On the privacy preserving properties of random data perturbation techniques. In: In Proceedings of the 3rd International Conference on Data Mining, pp 99–193

Li Y, Perlman E, Wan M, Yang Y, Meneveau C, Burns R, Chen S, Szalay A, Eyink G (2008) A public turbulence database cluster and applications to study lagrangian evolution of velocity increments in turbulence. J Turbul 9:N31, DOI 10.1080/14685240802376389

Liu Z, Adrian RJ, Hanratty TJ (2001) Large-scale modes of turbulent channel flow: transport and structure. J Fluid Mech 448:53–80, DOI 10.1017/S0022112001005808

Marchenko VA, Pastur LA (1967) Distribution of eigenvalues for some sets of random matrices. Mat Sb (NS) 72(114):507–536

Neal DR, Sciacchitano A, Smith BL, Scarano F (2015) Collaborative framework for piv uncertainty quantification: the experimental database. Accepted to Meas Sci Technol

Novara M, Scarano F (2013) A particle-tracking approach for accurate material derivative measurements with tomographic piv. Exp Fluids 54:1–12, DOI 10.1007/s00348-013-1584-5

Raben SG, Charonko J, Vlachos PP (2012) Adaptive gappy proper ortogonal decomposition for particle im-

age velocimetry data reconstruction. Meas Sci Technol 23:025,303

Ravindran S (2000) Reduced-order adaptive controllers for fluid flows using pod. J Sci Comput 15:457–478, DOI 10.1023/A:1011184714898

Scarano F (2003) Theory of non-isotropic spatial resolution in piv. Exp Fluids 35:26877

Schiavazzi D, Coletti F, Iaccarino G, Eaton JK (2014) A matching pursuit approach to solenoidal filtering of three-dimensional velocity measurements. J Comput Phys 263:206 – 221, DOI http://dx.doi.org/10.1016/j.jcp.2013.12.049

Sciacchitano A, Scarano F, Wieneke B (2012) Multi-frame pyramid correlation for time-resolved piv. Exp Fluids 53:1087105

Sirovich L (1987) Turbulence and the dynamics of coherent structures: I, ii, iii. Q Appl Math 45:561–590

Stewart G (2001) Matrix Algorithms Volume 2: Eigensystems, vol 2. Siam

Venturi D (2006) On proper orthogonal decomposition of randomly perturbed fields with applications to flow past a cylinder and natural convection over a horizontal plate. J Fluid Mech 559:215–254, DOI 10.1017/S0022112006000346

Venturi D, Karniadakis GE (2004) Gappy data and reconstruction procedures for flow past a cylinder. J Fluid Mech 519:315–336, DOI 10.1017/S0022112004001338

Violato D, Ianiro A, Cardone G, Scarano F (2012) Three-dimensional vortex dynamics and convective heat transfer in circular and chevron impinging jets. International Journal of Heat and Fluid Flow 37:22–36

Westerweel J (1994) Efficient detection of spurious vectors in particle image velocimetry data sets. Exp Fluids 16:23647

Westerweel J (1997) Fundamentals of digital particle image velocimetry. Meas Sci Technol 8:137992

Westerweel J (2000) Theoretical analysis of the measurement precision in particle image velocimetry. Exp Fluids 29:S312

Westerweel J, Scarano F (2005) Universal outlier detection for piv data. Exp Fluids 39:1096100

Westerweel J, Elsinga GE, Adrian RJ (2013) Particle image velocimetry for complex and turbulent flows. Annu Rev Fluid Mech 45:409–436

Yu H, Kanov K, Perlman E, Graham J, Frederix E, Burns R, Szalay A, Eyink G, Meneveau C (2012) Studying lagrangian dynamics of turbulence using on-demand fluid particle tracking in a public turbulence database. J Turbul 13:N12, DOI 10.1080/14685248.2012.674643